Journal of Superconductivity and Novel Magnetism (2021) 34:3395–3401
https://doi.org/10.1007/s10948-021-06043-1

ORIGINAL PAPER

Influence of Sintering Temperatures on the Phase Structure and Magnetic Properties of Spark Plasma Sintered $SmCo_5$ Magnets

Youwei Chen[1] · Qingzheng Jiang[1,2] · Xiang Li[1] · Sajjad Ur Rehman[1] · Chuanjia Zhao[1] · Jie Song[1] · Zhenchen Zhong[1]

Received: 25 August 2021 / Accepted: 21 September 2021 / Published online: 22 October 2021

Abstract

$SmCo_5$ magnets were prepared by spark plasma sintering (SPS) technique. The phase constitutions, magnetic properties, and microstructures of magnets prepared under different sintering temperatures were investigated systematically. It is observed that the 1:5 phase and 2:7 phase coexist in the magnet, and 2:17 phase appears when the temperature rises to 1050 °C. The best magnetic properties were obtained for the magnets prepared at 1000 °C, with remanence $J_r = 0.45$ T, intrinsic coercivity $H_{cj} = 985$ kA/m, and maximum energy density $(BH)_{max} = 37$ kJ/m^3. It is shown that the SPSed magnet prepared at 1000 °C exhibits excellent thermal stability which is described in terms of temperature coefficient of remanence (α) = −0.15%/°C and temperature coefficient of coercivity (β) = −0.25%/°C in the temperature range of 27–400 °C. The microstructure analysis showed that the high density of the magnet and the uniform distribution of the hard magnetic phase are the main reasons for the excellent magnetic properties.

Keywords $SmCo_5$ · Phase structure · Magnetic properties · Spark plasma sintered magnets

1 Introduction

As the first-generation rare earth permanent magnets, $SmCo_5$ magnet is attractive due to its high temperature application [1–4]. $SmCo_5$ is widely used in electric motors, generators, and transformers applications [5–8]. $SmCo_5$ magnet has not only high Curie temperature of 727 °C, but also a relatively high magnetic energy product [9–12]. Compared with Sm_2Co_{17} magnet and other SmCo-based magnets, $SmCo_5$ has larger magnetocrystalline anisotropy field of 31,840 kA/m [13, 14]. In addition, the corrosion resistance and high temperature stability of NdFeB are not as good as $SmCo_5$ [15, 16].

In order to obtain higher coercivity, high remanence and high temperature stability, it is necessary to further study the microstructure and phase composition of $SmCo_5$ [17, 18]. Xu et al. reported a new design of using Sm_2Co_7 nanophase to induce low-temperature hot deformation to prepare $SmCo_5$ magnets. The Sm_2Co_7 nanophase can promote the grain rotation and grain boundary sliding of the $SmCo_5$ phase, thereby coordinating the deformation of the two phases and avoiding local stress concentration, and finally obtaining a high coercivity magnet with good c-axis texture under low-temperature hot deformation [19]. Broad et al. found that the performance of $SmCo_5$ deteriorated mainly due to the easier nucleation of the reverse domain due to the precipitation of Sm_2Co_{17} [6]. Compared with conventional sintering, spark plasma sintering (SPS) is widely used in the fabrication of fully dense rare-earth permanent magnets with fine grain microstructure due to its short processing cycle and low sintering temperature [20–27]. Anas Eldosouky et al. reported that $SmCo_5$ SPSed magnet prepared at 900 °C shows improved performance compared to conventionally sintered (CVSed) magnets [26]. Liang et al. investigated the microstructure and magnetic properties of hot deformed $SmCo_5$ nanocrystalline magnet prepared from amorphous precursors, and the hot deformed $SmCo_5$ magnet depicted magnetic properties of $H_{cj} = 2450$ kA/m, $J_r = 0.64$ T, $(BH)_{max} = 804$ kJ/m^3, and the remanence

✉ Qingzheng Jiang
jqz666@126.com

✉ Zhenchen Zhong
zczhong2013@163.com

[1] Jiangxi Key Laboratory for Rare Earth Magnetic Materials and Devices & College of Rare Earths, Jiangxi University of Science and Technology, Ganzhou 341000, People's Republic of China

[2] Fujian Key Laboratory for Rare Earth Functional Materials, Longyan 366300, People's Republic of China

ratio of the magnet is as high as 0.87 due to the strong c-axis texture [27].

Hot-pressed precursors have a great influence on the microstructure and phase composition of the hot deformed magnets. However, recent works on the precursors of SPSed $SmCo_5$ hot deformation mainly focuses on the amorphous precursors [19, 27], but few crystalline precursors have been studied. In this work, SPSed $SmCo_5$ hot-pressed precursors were prepared at different sintering temperatures, and the correlation between the microstructure and magnetic properties are investigated systematically.

2 Experiment

The commercial quick-setting tablets with a nominal composition of $SmCo_5$ pulverized in a glove box to obtain powders were used as the original materials for SPSed magnets. The SPSed magnets were prepared at different sintering temperatures ranging from 900 to 1050 °C under a pressure of 50 MPa for 5 min with graphite mold. SPSed $SmCo_5$ magnet in cylindrical shape with a diameter of 15 mm and a height of about 7 mm were obtained. The optimized magnetic properties of the samples were obtained by adjusting the sintering temperature. The phase structures of SPSed magnets were characterized by X-ray diffraction (XRD) using Cu K_α radiation by a continuous scanning mode with a scan speed of 2.5°/min in the range of 20–90°. The XRD date was analyzed by Rietveld refinement method [28]. The room temperature (27 °C) performance of the magnets was measured by a B-H tracer (NIM-500C). Physical Property Measurement System (PPMS) equipped with a vibrating sample magnetometer (VSM) was applied to obtain the demagnetization curves in the temperature range 27 to 400 °C at a maximum magnetic field of 6 T. The morphology and elemental distribution of the selected magnets were observed by scanning electron microscopy (SEM).

3 Results and Discussion

Figure 1a displays the XRD patterns of the powder and the SPSed $SmCo_5$ magnets prepared at different sintering temperatures. The powder and all the SPSed magnets sintered at 900–1050 °C consist of 1:5 phase and 2:7 phase which is similar to the conventional sintered magnets [6, 20], but when the sintering temperature reaches 1050 °C, the peak strength of the 1:5 phase becomes weaker and 2:17 phase with Th_2Ni_{17}-type hexagonal crystal structure appears in the magnet. Figure 1b, c give the Rietveld refinement of XRD pattern of the magnet prepared at 1000 and 1050 °C, respectively. Table 1 gives the XRD refinement results for the magnets fabricated under 1000 and 1050 °C. The result shows that the 2:17 phase does exist in the magnet at the sintering temperature of 1050 °C. It is well established that the magnetic properties of SPSed $SmCo_5$ decrease by the formation of 2:17 phase [29]. In addition, Rietveld refinement was used to calculate the lattice constants which are given in Table 1. The refined results are in good agreement with the standard values of the 1:5 phase ($SmCo_5$, P6/mmm, a = 4.995 Å, c = 3.978 Å), 2:7 phase (Sm_2Co_7, R-3 m, a = 5.055 Å, c = 24.570 Å) and 2:17 phase (Sm_2Co_{17}, R-3 m, a = 8.402 Å, c = 12.172 Å) [30, 31].

Figure 2 gives the demagnetization curves of SPSed $SmCo_5$ magnets prepared under different sintering temperatures. Table 2 lists the values of the magnetic properties. The magnetic properties increase monotonically with the sintering temperature in the range of 900 to 1000 °C. The SPSed magnet prepared at the sintering temperature of 1000 °C shows the best intrinsic coercivity $H_{cj} = 985$ kA/m, remanence $J_r = 0.45$ T and maximum energy density $(BH)_{max} = 35$ kJ/m^3, respectively. On the one hand, as the temperature increases, the density of SPSed $SmCo_5$ magnets increases from 8.13 g/cm^3 at 900 °C to 8.40 g/cm^3 at 1000 °C and 1050 °C. On the other hand, when the temperature rises to 1050 °C, the performance of the magnet deteriorates due to the formation of 2:17 phase. The precipitated 2:17 phase acts as a reverse nucleation site, rather than domain wall pinning, and significantly reduce the coercivity [6].

Figure 3 depicts the demagnetization curves of the SPSed $SmCo_5$ magnet prepared at 1000 °C in the temperature range of 27–400 °C. The result shows that the magnetic properties decrease with the increase of temperature due to thermal demagnetization. Table 3 displays the detailed magnetic properties. The results show that the magnet exhibits stable magnetic properties at 200 °C, the intrinsic coercivity is 335 kA/m and remanence is 0.39 T. The stability of the magnetic properties can be evaluated by temperature coefficients of remanent magnetization (α) and temperature coefficient of coercivity (β). The temperature coefficient of the α and β of the magnets are −0.15%/°C and −0.25%/°C in the temperature range of 27–400 °C. The β value of SPSed $SmCo_5$ is better than that of conventional sintered $SmCo_5$ magnet [32], and it can be seen from Table 3 that the absolute value of β decreases with the increase of temperature, indicating the good temperature stability of SPSed $SmCo_5$ magnet.

The change in magnetic properties is due to the evolution of microstructures, so it is necessary to investigate the relationship between the magnetic properties and microstructure. Figure 4a–d gives the SEM BSE images of the section of SPSed magnets prepared at 900, 950, 1000, 1050 °C, respectively. The SPSed magnet prepared at 900 °C in the Fig. 4a shows a flaky section compared to the other dense magnets prepared at 950–1050 °C in the Fig. 4b–d, which corresponds to the lower density in Table 2, and explains

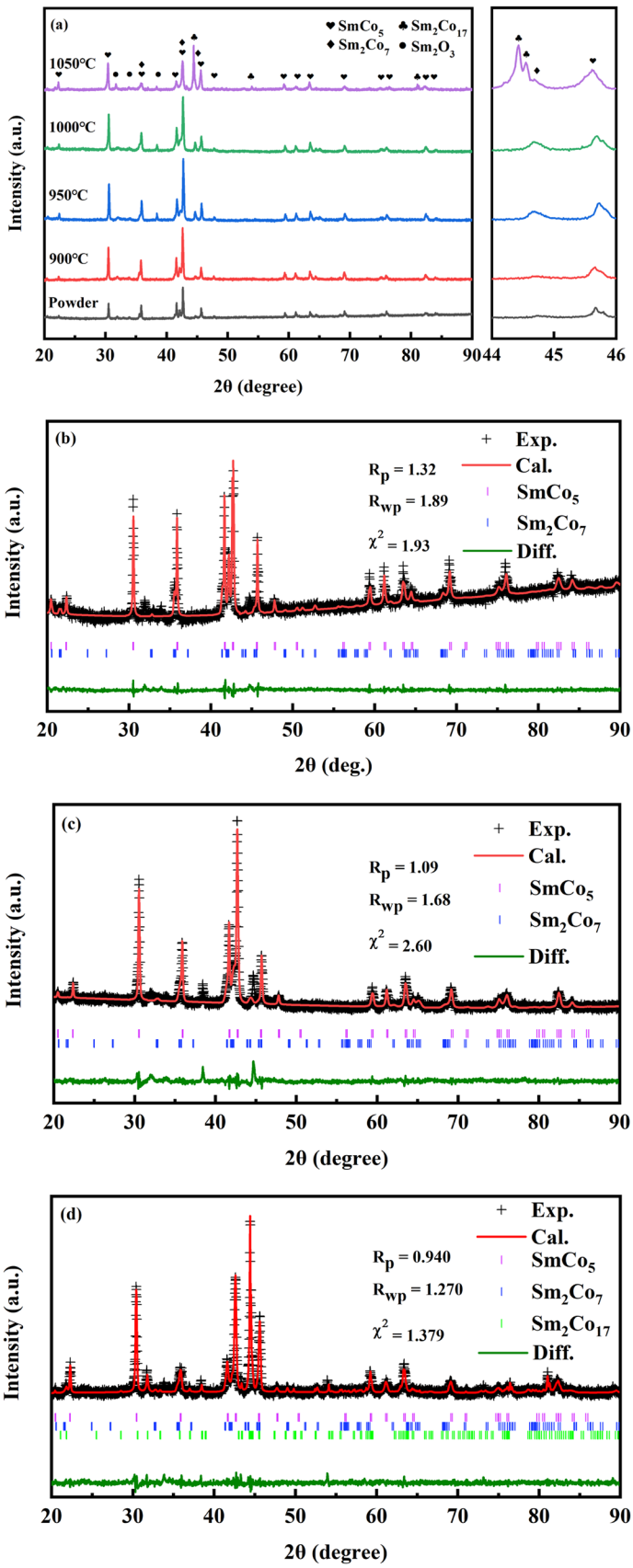

Fig. 1 **a** XRD spectrums of the $SmCo_5$ powder and the SPSed $SmCo_5$ magnets prepared under different sintering temperatures, (**b**), (**c**) and (**d**) the Rietveld refinement of XRD patterns of the $SmCo_5$ powder and the SPSed $SmCo_5$ magnets sintered at 1000 and 1050°C, respectively

Table 1 XRD refinement results for the powder and the SPSed $SmCo_5$ magnets prepared at 1000 and 1050 °C

Sample	Sintering temperature	1:5		2:7		2:17	
		a (Å)	c (Å)	a (Å)	c (Å)	a (Å)	c (Å)
Powder	/	4.998	3.975	5.057	24.570	/	/
SPSed Magnet	1000 °C	5.000	3.977	5.055	24.543	/	/
	1050 °C	4.999	3.982	5.054	24.552	8.399	12.178

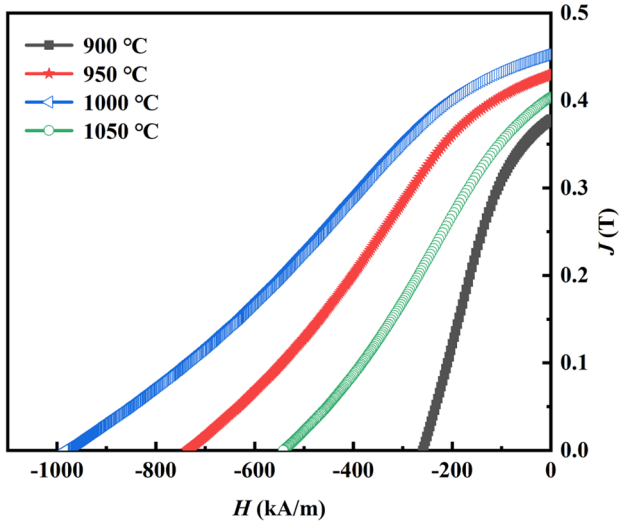

Fig. 2 Demagnetization curves of SPSed $SmCo_5$ magnets prepared under different sintering temperatures

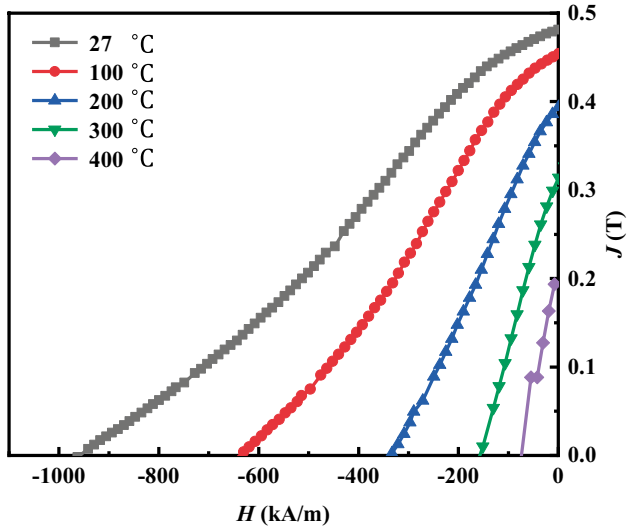

Fig. 3 Demagnetization curves of the SPSed $SmCo_5$ magnet (prepared under 1000 °C) as a function of temperature

the low magnetic performance obtained at 900 °C. However, when the temperature rises to 950 °C, the SPSed magnets show maximum density. Compared with the fracture morphology of the bulk $SmCo_5$ isotropic bonded magnet [33], the SPSed magnet is denser than bonded magnet and bonded magnet contains a lot of pores, which is also the main reason for the poor remanence. In order to further explore the relationship between performance and microstructure, the surface microstructure of the magnets was characterized by SEM in Fig. 5a–i.

In Fig. 5a, the microstructures of the initial powder consist of gray contrast, black contrast and the white spot around of the gray contrast. It is obvious that the gray contrast is uniformly and continuously distributed in the black contrast and it is very similar to the contrast distribution of the SPSed magnets prepared at 1000 °C in the Fig. 5b–e. The black dots marked by the red square in Fig. 5d are formed when the white dots fall off during polishing. While the microstructure of the magnet prepared at 1050 °C changed dramatically, as shown in Fig. 5f–i. The overall contrast is also composed of black contrast and gray contrast in Fig. 5f. However, the phase distribution is not uniform in general, and there are even phase agglomerations. Fig. 5g, h are partial enlargements of the left and right sides of Fig 5f, respectively. It can be observed that the phase distribution in Fig. 5g, h is

Table 2 The magnetic properties of the SPSed $SmCo_5$ magnets prepared under different sintering temperatures

Sintering temperatures (°C)	J_r (T)	H_{cj} (kA/m)	$(BH)_{max}$ (kJ/m^3)	ρ (g/cm^3)
900	0.38	260	19	8.13
950	0.43	738	30	8.36
1000	0.45	985	35	8.40
1050	0.40	542	23	8.40

Table 3 The high temperature magnetic properties of the SPSed $SmCo_5$ magnets prepared under 1000 °C

T (°C)	J_r (T)	H_{cj}(kA/m)	$(BH)_{max}$(kJ/m^3)	α (%/°C)	β (%/°C)
27	0.48	958	37	/	/
100	0.45	638	29	−0.08	−0.46
200	0.39	335	17	−0.11	−0.38
300	0.31	157	8	−0.13	−0.31
400	0.20	74	3	−0.15	−0.25

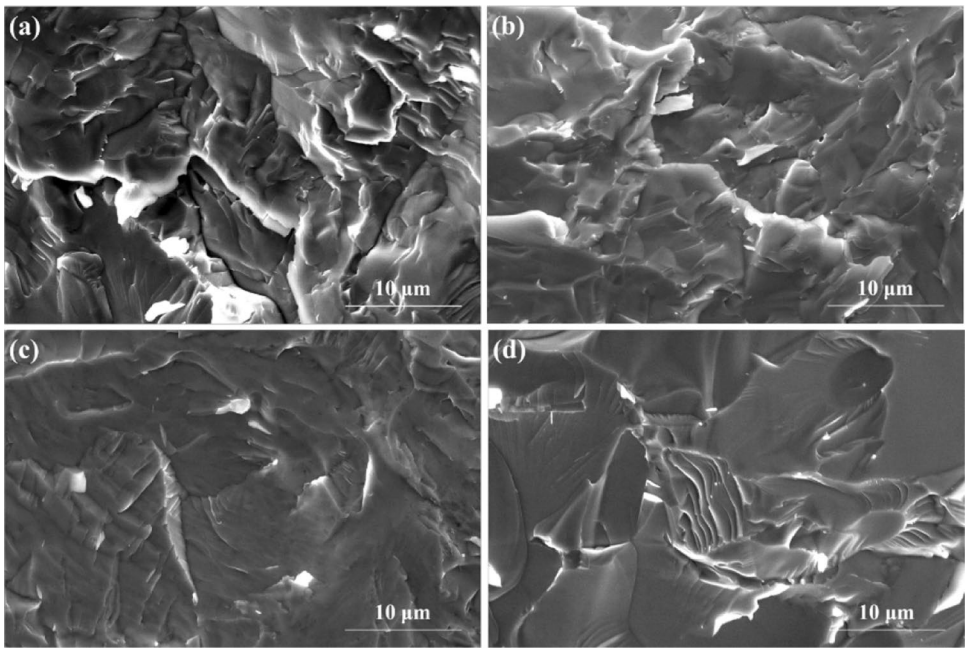

Fig. 4 Fracture morphology of the SPSed $SmCo_5$ magnet prepared at 900 °C (**a**), 950 °C (**b**), 1000 °C (**c**), and 1050 °C (**d**)

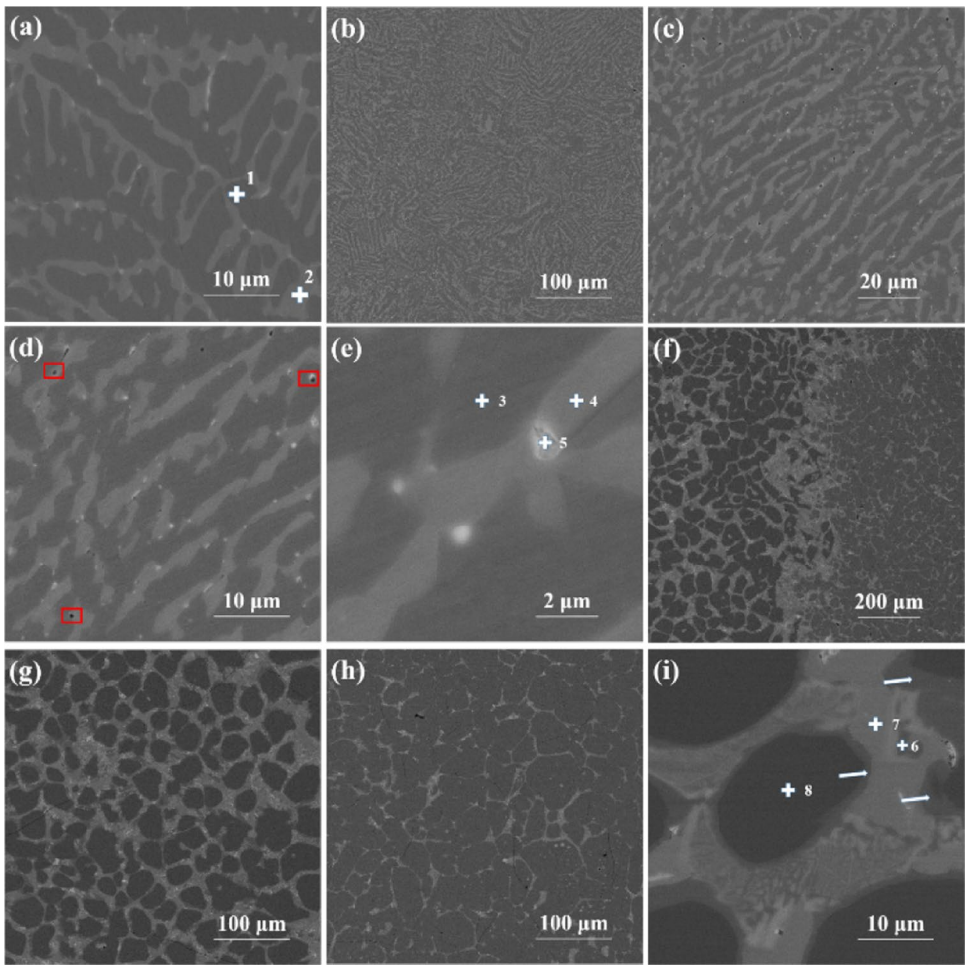

Fig. 5 **a**, **b**–**e** and **f**–**i** SEM BSE images of the initial powder, magnet prepared at 1000 °C and 1050 °C, respectively

Table 4 The composition of the sites marked in Fig. 5a, e, i

Site	Sm (at.%)	Co (at.%)	O (at.%)	Phases
1	17.91	82.09	/	$SmCo_{4.58}$ (1:5)
2	22.78	77.22	/	$SmCo_{3.38}$ (2:7)
3	16.4	83.6	/	$SmCo_{5.09}$ (1:5)
4	23.1	76.9	/	$SmCo_{3.33}$ (2:7)
5	39.7	/	60.3	Sm_2O_3
6	17.9	82.1	/	$SmCo_{4.59}$ (1:5)
7	23.2	76.8	/	$SmCo_{3.31}$ (2:7)
8	11.1	88.9	/	$SmCo_{8.01}$ (2:17)

somewhat similar to the core-shell structure in NdFeB [34]. The distribution of Fig. 5h is similar to that of Fig. 5g, but the gray contrast distribution is finer and the so-called shell structure is less complete than that in Fig. 5g. In order to further understand the contrast distribution in Fig. 5g, we enlarge Fig. 5g to get the Fig. 5i. And it can be seen that, in addition to the black contrast and the gray contrast, there is also a lighter black between the black contrast and the gray contrast in Fig. 5i, as shown by the white arrow and the white cross 6. The compositions of the selected contrasts were determined by EDS and summarized in Table 4. According to EDS results, it can be concluded that the black contrast in Fig. 5a–e is $SmCo_5$ main phase, the gray contrast is the second phase Sm_2Co_7 and the white dot is Sm_2O_3 phase. Compared with the SEM of traditional sintered $SmCo_5$, the main phase of the SPSed magnet presents a uniform and continuous strip, while the conventional sintered magnet presents an aggregated cluster [20]. Adsorbed oxygen on the metal powder leads to the formation of Sm_2O_3 in the $SmCo_5$ at high temperature [6, 20, 29]. Unlike the SPSed magnets prepared at 1000 °C, the black contrast of the so-called core structure in the magnets prepared at 1050 °C corresponds to the Sm_2Co_{17} phase. The gray contrast corresponds to Sm_2Co_7 and the lighter black contrast between those phases is $SmCo_5$. It is well known that in addition to the main phase of $SmCo_5$, the second phase of Sm_2Co_7 is generally present in $SmCo_5$ type magnets, but the appearance of Sm_2Co_{17} phase is rarely explained. Oxidation of samarium and evaporation at high temperatures may lead to the formation of 2:17 phase [6]. The oxidation of Sm cannot be completely avoided, but the precipitation of 2:17 phase can be prevented by controlling the content of Sm [35]. The observation of SEM and EDS matches well to the results of XRD and Rietveld refinement results.

The difference in the microstructure of the magnets prepared at 1000 and 1050 °C may be related to the sintering principle of SPS. The working process of SPS has three characteristics, including particle discharge, conductive heating and pressurization. In addition to the two traditional sintering methods, heating and pressurizing, which can promote sintering, the plasma generated by the discharge between the powder particles has a high temperature, which can cause local high temperatures on the surface of the particles [36, 37]. So, the temperature between particles may be far higher than 1050 °C. The temperature rise leads to the enhanced fluidity of the Sm-rich phase, resulting in the agglomeration of rare earth elements as shown in Fig. 5f and also leads to the growth of crystal grains and destroys the micro morphology.

4 Conclusions

In this paper, we systematically investigated the magnetic properties and microstructures of $SmCo_5$ spark plasma sintered magnets prepared at different sintering temperatures. When the sintering temperature ranges from 900 to 1000 °C, the phase of the magnet does not change according to the XRD and Rietveld refinement, and the increased density of the magnet is the key reason for the performance improvement. The optimal magnetic properties of $J_r = 0.45$ T, $H_{cj} = 985$ kA/m, $(BH)_{max} = 35$ kJ/m^3 were obtained by regulating the sintering temperature to 1000 °C. The SPSed magnet prepared at 1000 °C exhibits good high temperature stability and that the coercivity of the magnet is still 335 kA/m at 200 °C, the remanence is 0.39 T, α and β are −0.15%/°C and −0.25%/°C in the temperature range of 27–400 °C. The SPSed $SmCo_5$ magnet is mainly composed of 1:5 phase and 2:7 phase, but when the sintering temperature rises to 1050 °C, 2:17 phase appears. The uniform and continuous distribution of hard magnetic 1:5 phase and 2:7 phase is the reason for the excellent performance of SPSed magnets prepared at 1000 °C. However, when the magnet is sintered at 1050 °C, 2:17 phase appears and uneven distribution of hard magnetic phase results, which leads to the deterioration of magnetic properties.

Funding This work was supported by the Key Research and Development Program of Jiangxi Province (Grant No. 20201BBE51010), China Postdoctoral Science foundation (Grant No. 2020M682064), Postdoctoral Science foundation of Jiangxi Province (Grant No. 2020KY19), the Program of Qingjiang Excellent Young Talents of Jiangxi University of Science and Technology (No. JXUSTQJYX2020003), the Ph.D. Start-up Foundation of Jiangxi University of Science and Technology (Grant No. JXXJBS18052) and the project funded by the science and technology bureau of Ganzhou city (No. 204301000105).

References

1. Bian, L.P., Li, Y., Han, X.H., Cheng, J.Y., Qin, X.N., Zhao, Y.Q., Sun, J.B.: Effect of multi-element addition of Alnico alloying elements on structure and magnetic properties of $SmCo_5$-based ribbons. Phys. B. **531**, 1–8 (2020)

2. Landa, A., Söderlind, P., Parker, D., Åberg, D., Lordi, V., Perron, A., Turchi, P.E.A., Chouhan, R.K., Paudyal, D., Lograsso, T.A.: Thermodynamics of the $SmCo_5$ compound doped with Fe and Ni: an ab initio study. J. Alloy. Compd. **765**, 659–663 (2018)
3. Xue, Z.Q., Guo, Y.Q.: Correlation between valence electronic structure and magnetic properties in RCo_5 (R = rare earth) intermetallic compound. Chin. Phys. B. **25**, 063101 (2016)
4. Zhang, D.T., Cai, N.X., Zhu, R.C., Liu, W.Q., Yue, M.: Low-cost $Sm_{0.7}Y_{0.3}Co_5$ sintered magnet produced by traditional powder metallurgical techniques. Rare Met. **39**, 421–428 (2020)
5. Ma, Z.H., Zhang, T.L., Wang, H., Jiang, C.B.: Synthesis of $SmCo_5$ nanoparticles with small size and high performance by hydrogenation technique. Rare Met. **37**, 21–26 (2018)
6. Bartlett, R.W., Jorgensen, P.J.: Microstructural changes in $SmCo_5$ caused by oxygen, sinter-annealing and thermal aging. J. Less-Common Met. **37**, 21–34 (1974)
7. Gutfleisch, O., Willard, M.A., Brück, E., Chen, C.H., Sankar, S.G., Liu, J.P.: Magnetic materials and devices for the 21st century: stronger, lighter, and more energy efficient. Adv. Mater. **23**, 821–842 (2011)
8. Ding, J., McCormick, P.G., Street, R.: Structure and magnetic properties of mechanically alloyed Sm_xCo_{1-x}. J. Alloy. Compd. **191**, 197–201 (1993)
9. Gabay, A.M., Hu, X.C., Hadjipanayis, G.C.: Preparation of YCo_5, $PrCo_5$ and $SmCo_5$ anisotropic high-coercivity powders via mechanochemistry. J. Magn. Magn. Mater. **368**, 75–81 (2014)
10. Inomata, K., Shikanai, S., Horie, H., Fukui, K.: On strain and coercive force of RCo_5. Jpn. J. Appl. Phys. **12**, 565 (1973)
11. Kumar, K., Das, D., Wettstein, E.: High coercivity, isotropic plasma sprayed samarium-cobalt magnets. J. Appl. Phys. **49**, 2052–2054 (1978)
12. Kubis, M., Handstein, A., Gebel, B., Gutfleisch, O., Müller, K.H., Schultz, L.: Highly coercive $SmCo_5$ magnets prepared by a modified hydrogenation-disproportionation-desorption-recombination process. J. Appl. Phys. **85**, 5666–5668 (1999)
13. Suresh, K., Gopalan, R., Bhikshamaiah, G., Singh, A.K., Rao, D.V.S., Muraleedharan, K., Chandrasekaran, V.: Phase formation, microstructure and magnetic properties investigation in Cu and Fe substituted $SmCo_5$ melt-spun ribbons. J. Alloy. Compd. **463**, 73–77 (2008)
14. Song, J., Jiang, Q.Z., Rehman, S.U., He, L.K., Li, X., Chen, Y.W., Zhao, C.J., Zhong, Z.C.: Magnetic properties and microstructure of Sm-Co-Fe-Cu-Zr-Hf spark plasma sintered magnets. Phys. B. **605**, 412711 (2020)
15. Kündig, A.A., Gopalan, R., Ohkubo, T., Hono, K.: Coercivity enhancement in melt-spun SmCo5 by Sn addition. Scr. Mater. **54**, 2047–2051 (2006)
16. Jiang, Q.Z., Song, J., Huang, Q.F., Rehman, S.U., He, L.K., Zeng, Q.W., Zhong, Z.C.: Enhanced magnetic properties and improved corrosion performance of nanocrystalline Pr-Nd-Y-Fe-B spark plasma sintered magnets. J. Mate Sci Technol. **58**, 138–144 (2020)
17. Kohlmann, H., Hansen, T.C., Nassif, V.: Magnetic structure of $SmCo_5$ from 5 K to the Curie temperature. Inorg Chem. **57**, 1702–1704 (2018)
18. Pentón, A., Estévez, E., Lora, R., Espina-Hernández, J.H., Grossinger, R., Turtelli, R.S., Valor-Reed, A.: On the nature of the disordered microstructure in $Sm(Co, Cu)_5$ alloys with increasing Cu content. J. Alloys Compd. **429**, 343–347 (2007)
19. Xu, X.C., Li, Y.Q., Ma, Z.H., Yue, M., Zhang, D.T.: Sm_2Co_7 nanophase inducing low-temperature hot deformation to fabricate high performance $SmCo_5$ magnet. J. Scr. Mater. **178**, 34–38 (2020)
20. Zhang, D.T., Zhu, R.C., Yue, M., Liu, W.Q.: Microstructure and magnetic properties of $SmCo_5$ sintered magnets. Rare Met. **39**, 1295–1299 (2019)
21. Munir, Z.A., Anselmi-Tamburini, U., Ohyanagi, M.: The effect of electric field and pressure on the synthesis and consolidation of materials: a review of the spark plasma sintering method. J. Mater Sci. **41**, 763–777 (2006)
22. Jiang, Q.Z., He, L.K., Lei, W.K., Zeng, Q.W., Rehman, S.U., Zhang, L.L., Liu, R.H., Li, J.J., Ma, S.C., Zhong, Z.C.: Microstructure and magnetic properties of multi-main-phase Ce-Fe-B spark plasma sintered magnets by dual alloy method. J. Magn. Magn. Mater. **475**, 746–753 (2019)
23. Liu, S., Kang, N.H., Feng, L., Lee, S.H., Yu, J.H., Lee, J.G.: Anisotropic nanocrystalline Nd-Fe-B based magnets produced by spark plasma sintered technique. IEEE Trans. Magn. **51**, 1–4 (2015)
24. Rao, N.V.R., Gopalan, R., Raja, M.M., Chandrasekaran, V., Chakravarty, D., Sundaresan, R., Ranganathan, R., Honoa, K.: Structural and magnetic studies on spark plasma sintered $SmCo_5$/Fe bulk nanocomposite magnets. J. Magn. Magn. Mater. **312**, 252–257 (2007)
25. Xu, X.C., Zhang, H.G., Wang, T., Li, Y.Q., Zhang, D.T., Yue, M.: Local orientation texture analysis in nanocrystalline $Sm_{0.6}Pr_{0.4}Co_5$ magnet and $(SmCo_5)_{0.6}(PrCo_5)_{0.4}$ composite magnet with strong magnetic anisotropy. J. Alloys Compd. **699**, 262−267 (2017)
26. Eldosouky, A., Ikram, A., Mehmood, M.F., Xu, X., Šturm, S., Rožman, K.Ž, Škulj, I.: Using of SPS technique for the production of high coercivity recycled $SmCo_5$ magnets prepared by HD process. IEEE Trans. Magn. **7**, 1–4 (2016)
27. Liang, J.M., Yue, M., Zhang, D.T., Li, Y.Q., Xu, X.C., Li, H.J., Xi, W.: Anisotropic $SmCo_5$ nanocrystalline magnet prepared by hot deformation with bulk amorphous precursors. IEEE Trans. Magn. **54**, 1–1 (2018)
28. Rietveld, H.M.: A profile refinement method for nuclear and magnetic structures. J. Appl. Crystallogr. **2**, 65–71 (1969)
29. Broeder, F.J.A.D., Zijlstra, H.: Relation between coercive force and microstructure of sintered $SmCo_5$ permanent magnets. J. Appl. Phys. **47**, 2688–2695 (1976)
30. Andreev, A.V., Zadvorkin, S.M.: Thermal expansion and spontaneous magnetorestriction of RCo_5 intermetallic compounds. Phys. B. **172**, 517–525 (1991)
31. Sobolev, A.N., Golovnia, O.A., Popov, A.G.: Embedded atom potential for Sm–Co compounds obtained by forcematchin, J. Magn. Magn. Mater. **490**, 165468 (2019)
32. Yi, L., Sellmyer, D.J., Shindo, D.: Handbook of Advanced Magnetic Materials. Springer, US (2006)
33. Li, H.J., Wu, Q., Yue, M., Li, Y.Q., Zhuge, Y.T., Wang, D.J., Zhang, J.X.: Anisotropic nanostructured $SmCo_5$ bonded magnets fabricated by magneticfield-assisted liquid phase processing. J. Magn. Magn. Mater. **483**, 124–128 (2019)
34. Zhong, S.W., Yang, M.N., Rehman, S.U., Lu, Y.J., Li, J.J., Yang, B.: Microstructure, magnetic properties and diffusion mechanism of DyMg co-deposited sintered Nd-Fe-B magnets. J. Alloys Compd. **819**, 153002 (2020)
35. Ma, Q., Yue, M., Xu, X.C., Zhang, H.G., Zhang, D.T., Zhang, X.F., Zhang, J.X.: Effect of phase composition on crystal texture formation in hot deformed nanocrystalline $SmCo_5$ magnets. AIP Adv. **8**, 056214 (2018)
36. Chen, W., Anselmi-Tamburini, U., Garay, J.E., Groza, J.R., Munir, Z.A.: Fundamental investigations on the spark plasma sintering/synthesis process I. Effect of dc pulsing on reactivity. Mater. Sci. Eng. A. **394**, 132–138 (2005)
37. Anselmi-Tamburini, U., Gennari, S., Garay, J.E., Munir, Z.A.: Fundamental investigations on the spark plasma sintering/synthesis process II. Modeling of current and temperature distributions. Mater. Sci. Eng. A. **394**, 139–148 (2005)